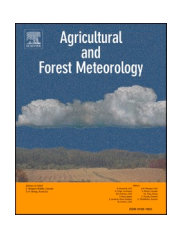
ELSEVIER

Contents lists available at ScienceDirect

Agricultural and Forest Meteorology

journal homepage: www.elsevier.com/locate/agrformet





Thermal property standards using granular media with air-pluviation and heat pulse probe measurements

Chihiro Dixon^a, Wenyi Sheng^{b,*}, Rong Zhou^a, Robert Horton^c, Scott B. Jones^a

- ^a Dept. of Plants, Soils and Climate, College of Agricultural and Applied Sciences, Utah State University, Logan, UT 84322-4820, USA.
- b Key Laboratory of Smart Agriculture System Integration, Ministry of Education, China Agricultural University, Beijing 100083, China
- ^c Dept. of Agronomy, Iowa State University, Ames, IA 50011-1051, USA.

ARTICLE INFO

Keywords: Thermal properties Granular media Heat pulse probe Air-pluviation

ABSTRACT

The fundamental thermal properties of soils and granular media include volumetric heat capacity (C_v), thermal conductivity (λ) and thermal diffusivity (κ), which play key roles in the transfer and maintenance of heat in the environment. Thermal properties are highly dependent upon the granular medium volumetric water content $(\theta_{\rm w})$, and thus thermal property functions are critical for modeling soil and land surface thermal processes. However, few available standard granular materials provide a source of 'known' thermal property values, perhaps foremost because of the difficulty in achieving a repeatable bulk density (ρ_b) value in addition to other packing and wetting complications. Our objectives were to identify and evaluate a range of readily available granular media that could be used to calibrate and validate thermal property measurements (i.e., Heat Pulse Probes, HPP) and to establish packing and wetting/draining methods that result in repeatable granular media conditions for thermal property determinations. We identified and tested a variety of granular media including spherical- (quartz sand, glass beads), angular- (crushed media) and aggregated- materials. Thermal property values were determined under uniform θ_w of oven-dried, saturated conditions and the drained-water content at -5.9 m suction using combined methods of HPP measurements for thermal property estimations and the multiple sieving pluviation (MSP) method, yielding highly repeatable ρ_b in coarse granular media. Overall, thermal property values ranged from 0.51 to 3.68 MJ m⁻³ K⁻¹ for C_{v_0} 0.13 to 3.73 W m⁻¹ K⁻¹ for λ and 0.17 to 1.5 mm² s^{-1} for κ . Optimized parameters were presented for selected $C_v(\theta_w)$ and $\lambda(\theta_w)$ thermal property models. We demonstrated that with the MSP method, it was possible to achieve highly repeatable $\rho_{\rm b}$ values and thermal property values for several commercially available granular materials. We recommend this approach as a standard calibration method based on 1) repeatable granular media packing and 2) standardized thermal property values for coarse granular media at targeted uniform θ_w distributions.

1. Introduction

Thermal properties, including volumetric heat capacity (C_v), thermal conductivity (λ), and thermal diffusivity (κ), are fundamental physical parameters. These properties are critical for understanding the Earth's energy balance, which affects vadose zone temperature-dependent processes such as microbial activity, redox potential, plant root uptake of water and nutrients, freezing and thawing processes as well as the transport of gasses, nutrients and water. Thermal properties in granular media vary with temperature, water content, pressure and mineral type (Farouki, 1981) as well as particle structural characteristics including

aggregation, bulk density (ρ_b), particle size distribution and particle shape (Dai et al., 2019). Therefore a number of thermal property models have been developed to characterize thermal properties by accounting for variable conditions. The mixing models developed by de Vries (1963) consider granular media as a constituent of solid, water, gas and organic matter, and the models are extensively used to characterize both C_v and λ at variable volumetric water contents (θ_w). Although the mixing model describing C_v is relatively straightforward and widely used, models describing λ continue to be developed to adequately describe the complexity of thermal conductance in three phases (i.e., solid, water and air). Numbers of λ models including the mixing model (Campbell et al.,

Abbreviations: HPP, Heat Pulse Probe; MSP, Multiple-Sieving Pluviation; ICPC, Identical Cylindrical Perfect Conductors; ILS, Infinite Line Sourse; THPP, Tri-needle Heat Pulse Probe.

E-mail address: wenyi.sheng@cau.edu.cn (W. Sheng).

^{*} Corresponding author.

1994; de Vries, 1963), empirical models (Campbell, 1985; Chung and Horton, 1987), the conceptual model (Lu and Dong, 2015) and the theoretical model (Ghanbarian and Daigle, 2016) are available with limitations for certain soil types and conditions. These models are often compared to thermal property measurements in field soils, while the application of thermal property models to readily available media is limited to quartz sand. The availability of standardized granular materials with well-characterized thermal property values (C_v , λ and κ) and the fitted parameters for available models can improve thermal property sensor calibration and performance and advance the development and validation of heat transfer models and their simulation capabilities.

The Dual-needle (also dual-rod) Heat Pulse (DHP) technique employed using Heat Pulse Probes (HPPs) is widely employed in science and engineering fields for determining thermal property values (Bilskie et al., 1998; Bristow et al., 1994; Noborio et al., 1996) and a variety of surrogate properties and processes such as water flux (Hopmans et al., 2002; Knight et al., 2012; Yang et al., 2013), subsurface evaporation rate (Heitman et al., 2008), heat flux (Cobos and Baker, 2003) and heat storage (Ochsner et al., 2007). An exsitensive review article for HPPs was provided by He et al., 2018. The HPP consists of a line source heater rod and at least one parallel temperature sensing rod. The measured and subsequently modeled temporal temperature rise generally yields all three available thermal property values via model fitting (i.e., $C_{\rm v}$, κ and λ). However, accuracy relies heavily on the determination of the center-to-center spacing, $r_{\rm c}$, between the temperature sensing rod (s) and the adjacent heater rod.

A widely used conventional model employed in HPPs considers the heater rod as an infinite line source (ILS) that outputs instantaneous heat (Campbell et al., 1991) or creates heat during a finite time interval (Bristow et al., 1994). This ILS model has been used as a standard method to measure thermal conductivity (ASTM International. Subcommittee D18. 12 on Rock Mechanic, 2008). However, the ILS model yields biased thermal property determination associated with the finite size and contrasting thermal properties of the heater- and temperature-sensing- rods (Guaraglia and Pousa, 1999; Hopmans et al., 2002). Additionally, recent designs of the HPP include thickened stainless-steel rods to minimize rod deflections, resulting in reduced thermal property value errors associated with rod spacing errors. Therefore, Knight et al. (2012) developed a model which includes the physical dimensions and the heat capacity of rod materials including stainless steel and filling epoxy. This semi-analytical model is called the "Identical Cylindrical Perfect Conductors (ICPC)" model and provides better estimations of thermal property values compared to those estimated by the ILS model for agar-stabilized water and air-free ice (Naruke et al., 2021) as well as for selected soil materials (i.e., sand and loam) (Peng et al., 2021) with known thermal properties.

Despite the wide application and development of HPPs, thermal property standards and measurement protocols using globally-available granular media have not been established. In-situ HPP calibration is traditionally conducted in agar-stabilized water, while Naruke et al. (2021) established the calibration protocol using air-free ice to provide additional standard properties. Various studies (Liu et al., 2013; Zhang et al., 2020) also explored on-site HPP calibration in the field. However, there is a gap between in-situ calibration in non-porous media and on-site calibration in heterogeneous field soils, and targeting commercially available granular media as standard calibration options can advance the development of thermal property sensors. Most manufacturers of granular media provide a single value of λ or sometimes include a range of λ values across a θ_w range from dry to wet, however, a reliably measured suite including all three fundamental thermal properties (C_{v} , λ and κ) is to our knowledge unavailable. A major challenge of developing a standardized in-situ method using granular media has included establishing and maintaining a repeatably- and accurately-packed material at different $\theta_{\rm w}$ conditions. Because $\rho_{\rm b}$ variation directly impacts solid- and pore space- configuration, it consequently impacts thermal properties. Suggesting a variety of readily-available granular media

exhibiting different mineral types (e.g., quartz and aluminum oxide), particle shapes (e.g., spherical and angular) and particle structures (e.g., aggregated and non-aggregated), may enable the advancement of our understanding of heat transport mechanism through different constituent phases (i.e., soild, water and air).

Traditionally, pluviation, tamping and vibration methods under dryor wet- conditions have been widely-used to prepare granular media in laboratory testing and field engineering studies and applications (Shi et al., 2021; Tabaroei et al., 2017). Air-pluviation uses a funnel to channel granular media at maintained velocity from a certain height (ASTM Committee D-18 on Soil and Rock., 2006) and is widely used to provide repeatable ρ_b (Kodicherla et al., 2018; Shi et al., 2021; Tabaroei et al., 2017). The early work by Miura and Toki (1982) first demonstrated the air-pluviation using a screen column, called the "Multiple Sieving Pluviation (MSP)" method, allowing particles to scatter randomly while pouring media into a column, preventing particle segregation. Shi et al. (2021) evaluated the homogeneity and microstructure of granular media prepared by air- and water- MSP methods and moist- and dry- tamping methods of coarse calcareous sand and showed that the air-MSP method provided the highest homogeneity. Both tamping and vibration are often combined with the MSP method, and Yu et al. (2006) demonstrated that properly controlled vibration results in disordered to ordered packing and the highest ρ_b . However, the denser packing using the vibration method for ellipsoidal-shaped particles can alter particle orientation (e.g., horizontal or vertical) and exhibits a wall effect (Gan and Yu, 2020), meaning that the vibration method alters particle contact and the contact between HPP rods and ellipsoidal-shaped particles. Given the theoretical assumptions for heat transport in homogeneously packed granular media, we find the air-MSP method to be a critical standard preparation method for HPP calibration measurements for repeatable thermal property measurements in coarse granular packed media.

Our objectives were to 1) determine the repeatability of coarse granular media packing density using the MSP method, 2) to determine the HPP-based thermal properties of these media using the ICPC model at oven-dried-, saturated- and drained- θ_w conditions, and 3) to determine model parameter values describing θ_w -dependent C_v and λ values of these media based on fitted data.

2. Theory

2.1. ICPC model

Knight et al. (2012) presented the ICPC model, which is a semi-analytical solution of the temperature rise with time, $\Delta T(t)$ at a known distance from the line-source heater, $r_{\rm c}$ (m), as the heat propagates through a homogeneous and isotropic medium. The Laplace transform solution of this process is written as:

$$\widehat{T}_{C}(\mathbf{p}) = \frac{q' K_{0}(\mathbf{\mu} r_{c})}{2\pi \lambda \mathbf{p} \left\{ \mathbf{\mu} a_{0} \left[K_{1}(\mathbf{\mu} a_{0}) + \left(\frac{\mathbf{\mu} a_{0} \beta_{0}}{2} \right) K_{0}(\mathbf{\mu} a_{0}) \right] \right\}^{2}}$$
(1)

where q' represents the heat input (W m $^{-1}$), p is the Laplace transform variable (s^{-1}) and $\widehat{T}_{\rm C}(p)$ is the Laplace transform of the temperature arriving at the sensing rod, $T_{\rm C}(t)$, for the case of continuous heating. Also, $K_{\rm n}(z)$ is the modified Bessel function of the second kind of order n and argument z, $\mu = \sqrt{p/\kappa}$, a_0 is the radius of the rod (m), $\beta_0 = C_0/C_{\rm v}$. The weighted average volumetric heat capacity of the rod, C_0 , including stainless steel and epoxy was calculated as:

$$C_0 = C_E \frac{d_E^2}{d_0^2} + C_{SS} \left(1 - \frac{d_E^2}{d_0^2} \right)$$
 (2)

where C_E and C_{SS} are volumetric heat capacities of rod-epoxy and -stainless-steel and d_E and d_0 are the inner and outer diameters of the stainless-steel rod, respectively. Based on the principle of superposition,

the temperature increase from a heating pulse can be calculated as:

$$\Delta T(t) = \begin{cases} \Delta T_C(t) & 0 < t \le t_0 \\ \Delta T_C(t) - \Delta T_C(t - t_0) & t > t_0 \end{cases}$$
(3)

where t is the elapsed time (s) and t_0 is a short duration of heat input (s), which conventionally is 8 s. This solution accounts for a finite rod radius and the finite heat capacity of both heater- and temperature-sensing-rods, including the stainless-steel tubing and the epoxy. The ICPC model becomes identical to the traditional line-heat source (ILS) model (also referred to as Pulsed Infinite Line Source or PILS) developed by Bristow et al. (1994) if the radius of both heater- and temperature-sensing-rod become zero ($a_0=0$). The introduction of finite rod radius (a_0) and a_0 0 account for the shift of heat-pulse arrival at the temperature-sensing-rods relative to the ILS model, reducing the bias of thermal property estimation in materials with a varied range of thermal properties.

2.2. Thermal property models

2.2.1. Volumetric heat capacity

The volumetric heat capacity of granular materials characterizes the amount of heat stored in a unit volume of media, which is an important characteristic determining the magnitude of annual and diurnal variations in heat storage impacting various processes. Since granular media primarily consists of minerals, water, air, and organic matter, C_v can be estimated from constituent-mass fractions and -specific heat capacities as follows (Campbell, 1985; de Vries, 1963):

$$C_{v} = \sum \rho_{x} c_{x} \theta_{x} \tag{4}$$

where ρ_x is constituent density (kg m⁻³), c_x is constituent specific heat capacity (MJ kg⁻¹ K⁻¹) and θ_x , is constituent volume fraction (m³ m⁻³). The subscript x specifies the mixture constituency where s, w, a, and om refer to solid, water, air, and organic matter, respectively. The solid-phase term may include multiple minerals such as quartz (q) and other minerals (m), and θ_s is the sum of the volume fraction weighted heat capacities of all identified minerals (i.e., $\theta_s = \theta_q + \theta_m$). Eq. (4) can be simplified if the air and organic matter terms are ignored due to their small heat capacity and small volume fraction, respectively (Bristow, 1998; Campbell, 1985).

2.2.2. Thermal conductivity

Thermal conductivity is the amount of heat transmitted through a unit area in a unit time under a unit temperature gradient, which varies with pore structure, temperature, water content, and mineral type in granular materials. Various λ functions of $\theta_{\rm W}$ have been proposed to characterize heat transfer through granular media, as Dong et al. (2015) discussed.

2.2.2.1. Mixing model. The 'mixing model' computes λ of a granular medium as a weighted sum of the thermal conductivities of material constituents (Campbell et al., 1994; de Vries, 1963):

$$\lambda(\theta_{\rm w}) = \frac{\sum k_x \theta_x \lambda_x}{\sum k_x \theta_x} \tag{5}$$

where again x specifies the mixture constituency and k_x is a constituent weighting factor. The organic matter component in Eq. (5) is normally combined with the solid phase for simplicity (de Vries, 1963), and if that is the case, the solid phase term in the equation is a comprehensive term that includes minerals and organic matter (i.e., s = q + m + om). The solid phase thermal conductivity term (λ_s) may include multiple minerals, e.g., quartz, mica, and others, which may require additional λ and k inputs for mixing models of C_v (Eq. (4)) and λ (Eq. (5)). The weighting factor, k_x , can be calculated as:

$$k_{x} = \frac{1}{3} \left[\frac{2}{1 + g_{a}(\lambda_{x}/\lambda_{f} - 1)} + \frac{1}{1 + g_{c}(\lambda_{x}/\lambda_{f} - 1)} \right]$$
 (6)

where g_a and g_c are shape factors, and λ_f is fluid thermal conductivity. Shape factors, g_a and g_c can be expressed as $g_a=0.088$ for mineral sand (Bittelli et al., 2015) and $g_c=1-2$ g_a , respectively. The thermal conductivity of air (λ_a) is the sum of the conductivity of dry air ($\lambda_{da}=0.025$ W m^{-1} K⁻¹, de Vries (1963)) and a vapor component associated with latent heat transfer. Campbell et al. (1994) introduced λ_f and an empirical function of water content, f_w , to simplify the k_x calculation in each constituent:

$$\lambda_f = \lambda_a + f_{\mathbf{w}}(\lambda_{\mathbf{w}} - \lambda_{\mathbf{a}}) \tag{7}$$

$$f_w = \frac{1}{1 + (\mathbf{\theta}_w/\mathbf{\theta}_0)^{-q}} \tag{8}$$

where θ_0 and q are material properties that affect the slope of the λ function, especially during the transition from the air- to the water-dominated stage. Bittelli et al. (2015) established linear regression models, $\theta_0=0.33\theta_c+0.078$ and $q=7.25\theta_c+2.52$, both of which are highly related to the clay content (θ_c). In this study, we assumed $\theta_c=0$ because our testing media were coarse-textured, therefore both parameters were constants with $\theta_0=0.078$ and q=2.52, respectively.

2.2.2.2. Campbell (1985) model. The following empirical $\lambda(\theta_w)$ model was developed by Campbell (1985):

$$\lambda(\boldsymbol{\theta}_{\mathbf{w}}) = A + \boldsymbol{B}\boldsymbol{\theta}_{\mathbf{w}} - (\boldsymbol{A} - \boldsymbol{D})\exp[-(\boldsymbol{C}\boldsymbol{\theta})^{E}]$$
(9)

where A, B, C, D and E are coefficients that can be determined by fitting Eq. (9) to the measured λ as a function of $\theta_{\rm w}$, or computed using the volume fraction constituents such as solid (s), quartz (q), other minerals (m) and clay (c) as follows.

$$A = \frac{0.57 + 1.73\theta_q + 0.93\theta_m}{1 - 0.74\theta_q - 0.49\theta_m} - 2.8\theta_s(1 - \theta_s), \quad B = 2.8\theta_s,$$

$$C = 1 + 2.6\theta_c^{-0.5}, \quad D = 0.03 + 0.7\theta_s^2, \quad E = 4$$
(10)

The λ value at saturation ($\theta_{\rm sat}$) can be calculated as $\lambda(\theta_{\rm sat})=A+B\theta_{\rm sat}$, and we determined the A and B values by fitting Eq. (10) to λ measurements. The coefficient C determines how the curve rapidly increases in the lower range of $\theta_{\rm w}$. Although our coarse granular media did not include clay, C=1 leads to a linear λ function of $\theta_{\rm w}$ with no transition point. Therefore, we set C=83, representing a very small clay content, $\theta_{\rm c}=0.001$. The D value represents the λ value when $\theta_{\rm w}=0$, therefore and D was computed as an average of oven-dry λ measurements.

2.2.2.3. Chung and Horton (1987) model. An empirical model developed by Chung and Horton (1987) is described as

$$\lambda(\boldsymbol{\theta}_{\mathbf{w}}) = \boldsymbol{b}_1 + \boldsymbol{b}_2 \boldsymbol{\theta}_{\mathbf{w}} + \boldsymbol{b}_3 \boldsymbol{\theta}_{\mathbf{w}}^{0.5} \tag{11}$$

where b_1 , b_2 and b_3 are empirical parameters determined for specific soils. The parameter, b_1 refers to the oven-dry λ ($\lambda_{\rm dry}$) when $\theta_{\rm w}=0$. Chung and Horton (1987) reported parameters b_1 , b_2 and b_3 for three soil types (i.e., sand, silt and clay).

2.2.2.4. Lu and Dong (2015) model. Lu and Dong (2015) developed a $\lambda(\theta_{\rm W})$ model similar to the sigmoidal function of the water retention curve developed by van Genuchten (1980), the retention curve being the relationship between $\theta_{\rm W}$ and the matric potential of the media. The Lu and Dong (2015) model included an onset of the thermal conductivity function $\theta_{\rm Wf}$ and a fluid network connectivity parameter, m.

$$\frac{\lambda(\theta_{w}) - \lambda_{dry}}{\lambda_{sat} - \lambda_{dry}} = 1 - \left[1 + \left(\frac{\theta_{w}}{\theta_{wf}}\right)^{m}\right]^{1/m-1}$$
(12)

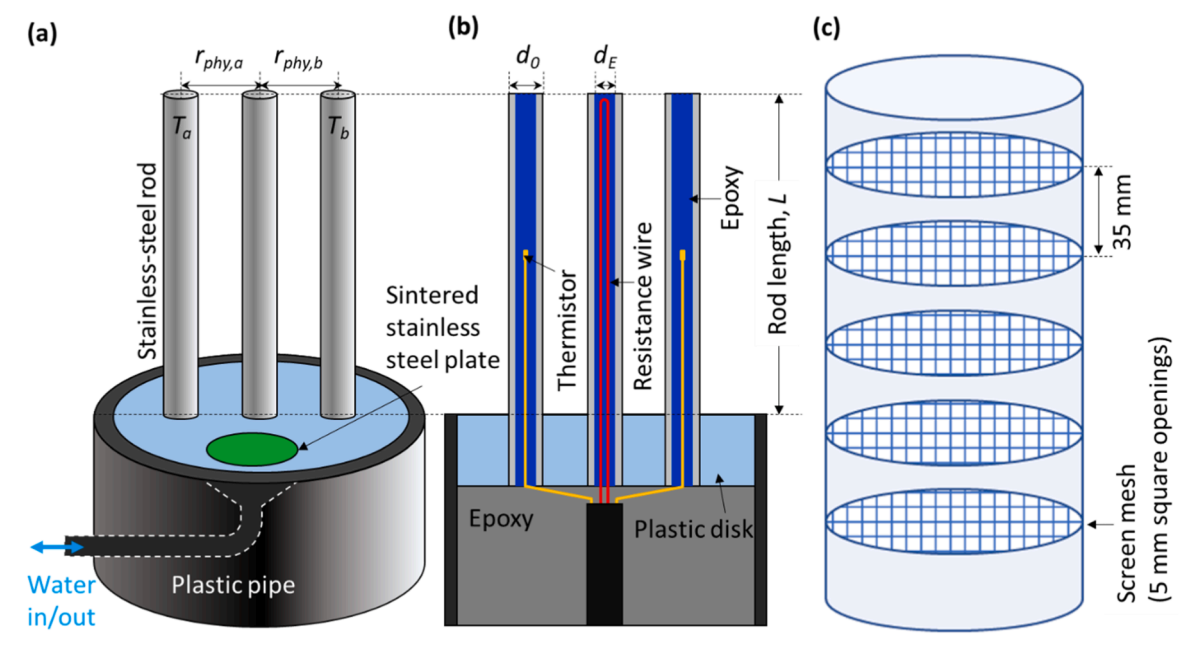


Fig. 1. (a) A pictorial drawing of THPP, (b) a cross-sectional pictorial drawing of THPP and (c) a pictorial drawing of a layered screen column.

2.2.2.5. Ghanbarian and Daigle (2016) model. Ghanbarian and Daigle (2016) developed a theoretical λ model using the percolation-based effective-medium approximation:

$$(\boldsymbol{\theta}_{sat} - \boldsymbol{\theta}_{w}) \frac{\boldsymbol{\lambda}_{dry}^{1/t_{s}} - \boldsymbol{\lambda}^{1/t_{s}}}{\boldsymbol{\lambda}_{dry}^{1/t_{s}} + [(\boldsymbol{\theta}_{sat} - \boldsymbol{\theta}_{wc})/\boldsymbol{\theta}_{wc}] \boldsymbol{\lambda}^{1/t_{s}}} + \boldsymbol{\theta}_{w} \frac{\boldsymbol{\lambda}_{sat}^{1/t_{s}} - \boldsymbol{\lambda}^{1/t_{s}}}{\boldsymbol{\lambda}_{sat}^{1/t_{s}} + [(\boldsymbol{\theta}_{sat} - \boldsymbol{\theta}_{wc})/\boldsymbol{\theta}_{wc}] \boldsymbol{\lambda}^{1/t_{s}}} = 0$$

$$(13)$$

where $t_{\rm S}$ is the scaling factor. The critical water content, $\theta_{\rm wc}$, is the volumetric water content at which the liquid phase first forms a continuous path through the porous medium. Ghanbarian and Daigle (2016) described the $\theta_{\rm wc}$ value as analogous to the parameter $\theta_{\rm wf}$ in the Lu and Dong (2015) model. The Ghanbarian and Daigle (2016) model is especially flexible to fit a variety of porous media, especially fine-textured soils, and Sadeghi et al. (2018) suggested various existing models are special cases of Ghanbarian and Daigle (2016). While Eq. (12) is an implicit λ function, Sadeghi et al. (2018) derived an explicit λ form as follows:

$$\lambda(\theta_{w}) = \left[a_{1} + a_{2}\theta_{w} + sgn(t_{s})a_{2}\sqrt{b_{3} + 2b_{1}b_{2}^{-1}\theta_{w} + \theta_{w}^{2}}\right]^{t_{s}}$$
(14)

$$a_{1} = \frac{-\theta_{c}\lambda_{sat}^{1/t_{s}} + (\theta_{sat} - \theta_{wc})\lambda_{dry}^{1/t_{s}}}{2(\theta_{sat} - \theta_{wc})}, a_{2} = \frac{\lambda_{sat}^{1/t_{s}} - \lambda_{dry}^{1/t_{s}}}{2(\theta_{sat} - \theta_{wc})},$$

$$a_{3} = \frac{\left[\theta_{wc}\lambda_{sat}^{1/t_{s}} - (\theta_{dt} - \theta_{wc})\lambda_{dry}^{1/t_{s}}\right]^{2} + 4\theta_{wc}(\theta_{sat} - \theta_{wc})\lambda_{sat}^{1/t_{s}}\lambda_{dry}^{1/t_{s}}}{\left(\lambda_{sat}^{1/t_{s}} - \lambda_{dry}^{1/t_{s}}\right)^{2}}$$
(15)

where sgn is the sign function (i.e., sgn(x > 0) = 1, sgn(x < 0) = -1).

2.3. Accuracy of thermal property estimations

The accuracy of thermal property estimates in granular media was evaluated using Root Mean Square Error (RMSE), which is often used in thermal properties analysis (He et al., 2017; Lu et al., 2019, 2014; Peng et al., 2019; Tian et al., 2016) written as:

$$RMSE = \sqrt{\frac{\sum (A_{cal} - A_{ref})^2}{n}}$$
 (16)

where A is the thermal property with lowercase "cal" and "ref" representing the calculated values using the listed models (Eqs. (4-15)) and the estimated values by fitting the ICPC model (Eqs. (1-3)) to HPP temperature rise with time measurements. The parameter n is the number of measurements. The RMSE provides knowledge of how far/close calculated thermal property values ($A_{\rm cal}$) are from the estimated thermal property values ($A_{\rm ref}$) based on measurements.

3. Materials and methods

3.1. Heat pulse probe construction

A Tri-needle Heat Pulse Probe (THPP) was constructed following the description of Naruke et al. (2021). The THPP consisted of three stainless steel rods (316 stainless steel, McMaster-Carr, Douglasville, GA, USA). Each of the two temperature-sensing-rods, T_a and T_b , contained a single thermistor (10K3MCD1, BetaTherm Corp., Shrewsbury, MA, USA) positioned at the rod's mid-length. The heater rod, positioned between the temperature rods, contained heater wire made from 40-gage enameled Nichrome resistance wire (Nichrome 80, Pelican Wire Co., Naples, FL, USA) with a constant resistance per wire length (221.9 Ω m $^{-1}$). The heater wire was folded in half to create a loop at the distal end of the rod. The heater- and thermistor- rods were filled with a thermally conductive epoxy (slow cure silver epoxy, Arctic Silver Inc., Visalia, CA, USA).

Fig. 1a shows a THPP with rods extending from the THPP base, and Fig. 1b shows the cross-section of the THPP. Table 2 describes the stainless-steel rod dimensions, including the physical rod spacing $(r_{\rm phy})$ between each thermistor-rod and the heater-rod, the length of rods (L) and outer- and inner- diameters of the rods, d_0 and $d_{\rm e}$, respectively. In

Fig. 1a, a 39 mm diameter polycarbonate disk of 10 mm thickness was drilled out to house the two thermistor-rods on either side of the heater-rod with a 7 mm center-to-center spacing between each rod pair. The plastic disk with a relatively small λ was used to avoid non-granular media-related heat transfer between rods, which could result in thermal property errors. A hole with a diameter of 1.5 cm was also drilled on the disk to attach a sintered stainless-steel plate connected to plastic tubing to infuse/withdraw water in the testing media. The heater- and thermistor- rod wires protruding from the bottom of the disk, as well as the tubing connected to the sintered stainless-steel disk, were potted inside

Table 1 Particle- and bulk densities (ρ_s and ρ_b), porosity (= 1 – ρ_b / ρ_s) and quartz (S_iO_2) fraction of granular media.

Name	Abbreviation	$_{\rm kg~m^{-3}}^{\rho_{\rm s}}$	$ ho_{ m b}$ kg m $^{-3}$	Porosity	SiO ₂ fraction				
Spherical granular media									
Fine sand	C778	2653	1829	0.31	0.95 –				
		± 8.55	± 1.77		0.99 ^{‡‡}				
Wedron sand	Wed	2674	1744	0.35	0.99				
		± 17.3	± 1.24						
Soda-lime	Sod	2500^{\dagger}	1556	0.38	$0.65 - 0.75^{\dagger}$				
glass beads			± 1.78						
	An	gular granul	ar media						
Coarse angular	Ang	2637	1607	0.39	0.9^{\ddagger}				
sand		± 11.0	± 0.84						
Aluminum	Alu	4019	1995	0.50	0.007				
Oxide		± 16.8	± 2.27		(Al ₂ O ₃				
					0.96)#				
Coal slag	Coa	2776	1616	0.42	0.41 –				
		± 45.6	± 1.65		$0.53^{\dagger\dagger}$				
Garnet	Gar	3900	2205	0.43	n/a				
		± 8.67	± 1.30						
	Aggr	egated gran							
Profile	Pro	2525	693	0.73	0.74				
		± 12.1	± 4.18						
Pumice	Pum	1718	488.3 \pm	0.72	n/a				
		± 28.3	1.17						

 $^{^\}dagger$ Mo-sci (2020): https://mo-sci.com/wp-content/uploads/product-docs/glass-microspheres/GL0191-Data-Sheet.pdf;

Table 2 Calibrated apparent rod spacing in agar-stabilized water (r_c) and thermistor rod dimensions and volumetric heat capacities of the THPP components (after Naruke et al. (2021)).

	Calibration	Thermistor rod dimension				Volumetric heat capacity		
	$r_{ m c}$	$r_{ m phy}$	L	d_0	$d_{ m e}$	$C_{\rm SS}$	$C_{\rm E}$	C_0
	mm						MJ m ⁻³	$^{3} K^{-1}$
T_a	6.96	6.87	50	2.4	0.61	4	2.03	3.87
Ть	6.96	6.94	"	"	"	"	"	"

of a 40 mm-i.d. ABS pipe using a two-part potting epoxy (50-3100RBKresin, CAT.150CL13-hardener, Epoxies, Etc., Cranston, RI, USA), where the polycarbonate disk was previously glued into the upper end of the pipe. The outer wall of the ABS pipe had two groves machined at the upper end to house O-rings for sealing against a 150 mm long, 57 mm i. d. clear Lexan tube used to contain the granular media. The distance between each thermistor-rod and the tube wall should exceed more than the r_{phy} value (i.e., 7 mm) to prevent the effect of different thermal property interfaces (i.e., granular media and air) (Kluitenberg and Philip, 1999). Our measurement system provided a sufficient distance (i.e., 18 mm) between the thermistor-rod and the wall. The heater wire of the THPP was connected in series with a 1- Ω precision resistor ($\pm 1\%$, 2 W), the voltage across which was measured by a CR6 datalogger (Campbell Scientific, Logan, UT, USA) for heating power calculation. The heating duration was 8 s with an average heating rate of $50.1 \pm 0.32 \,\mathrm{W m}^{-1}$. The thermistors were measured directly through the differential channels on the datalogger using the built-in 5-k Ω resistor ($\pm 0.1\%$, 10 ppm $^{\circ}$ C⁻¹) to complete the bridge. Thermistor temperatures were recorded for over

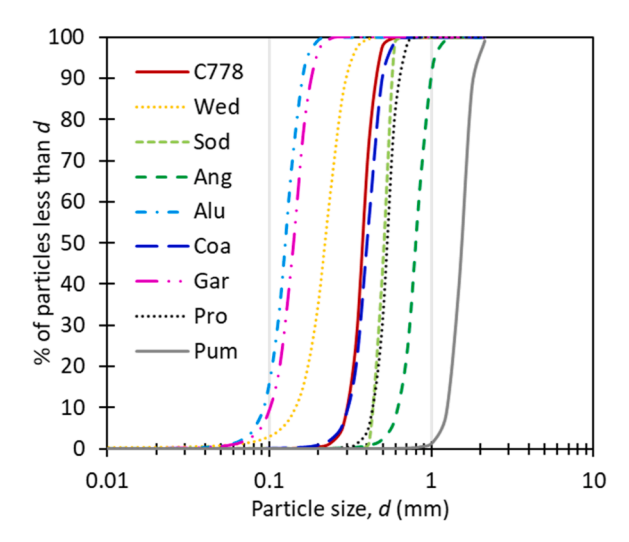


Fig. 2. Particle size distribution of coarse granular media. based on the parameters shown in Table 3.

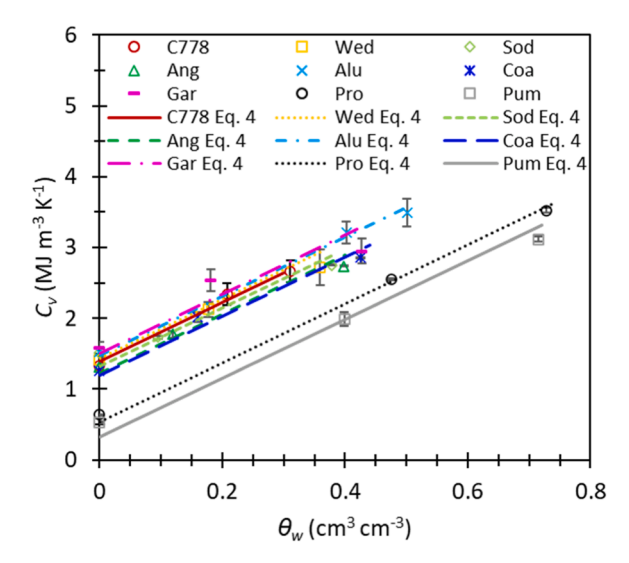


Fig. 3. The volumetric heat capacity (C_v) function of water content determined by THPP (symbols) and the mixing model (lines) using the fitted parameter shown in Table 5 . The standard deviation of estimated C_v by THPP measurements was shown as solid black bars.

150 (or 270) s, including 30 s prior to firing the heater, and a continuation for 120 (or 240) s to capture the heating peak, especially in dry granular media. Due to the large porosity and small λ of oven-dried pumice, a 30 + 240 s temperature rise with time data collection was needed to capture the temperature rise peak. The average pre-heating temperature for 5 s before the heat pulse initiation was used as the initial temperature. The 120 (or 240) s of heating and post-heating temperature data were used to optimize thermal properties using the ICPC model. Measurements were initiated every 20 min so the sample's temperature around the THPP could cool back down to near ambient temperature after heating to avoid temperature buildup or artificial thermal gradients. The temperature response and heating rate data were recorded for post-analysis of $r_{\rm c}$ and thermal properties.

3.2. Granular materials as reference media

Granular materials were selected to provide a wide range of thermal and physical properties as reference standards for HPP calibration and validation. The granular media included (a) spherical granular media:

[‡] Unimin (2020): https://www.coviacorp.com/media/dquhr5ed/granusil_tds_emmett_026_0719_bld_eng.pdf#search=granusil%202075

[§] Wedron Silica (2020): https://www.smooth-on.com/tb/files/WedronSilica. pdf; Profile (2020): http://www.profileevs.com/resources/article/greens-grade-emerald-standard-specifications;.

[#] Washintonmills (2020): https://www.washingtonmills.com/products/brown-fused-aluminum-oxide;

^{††} Blackbeauty (2020): https://www.blackbeautyabrasives.com/application/files/2015/8644/1909/SDS Original BLACK BEAUTY Jan 2020.pdf;

 $^{^{\}ddagger \ddagger}$ US Silica (2020): https://www.ussilica.com/support/guides-working-s afely.

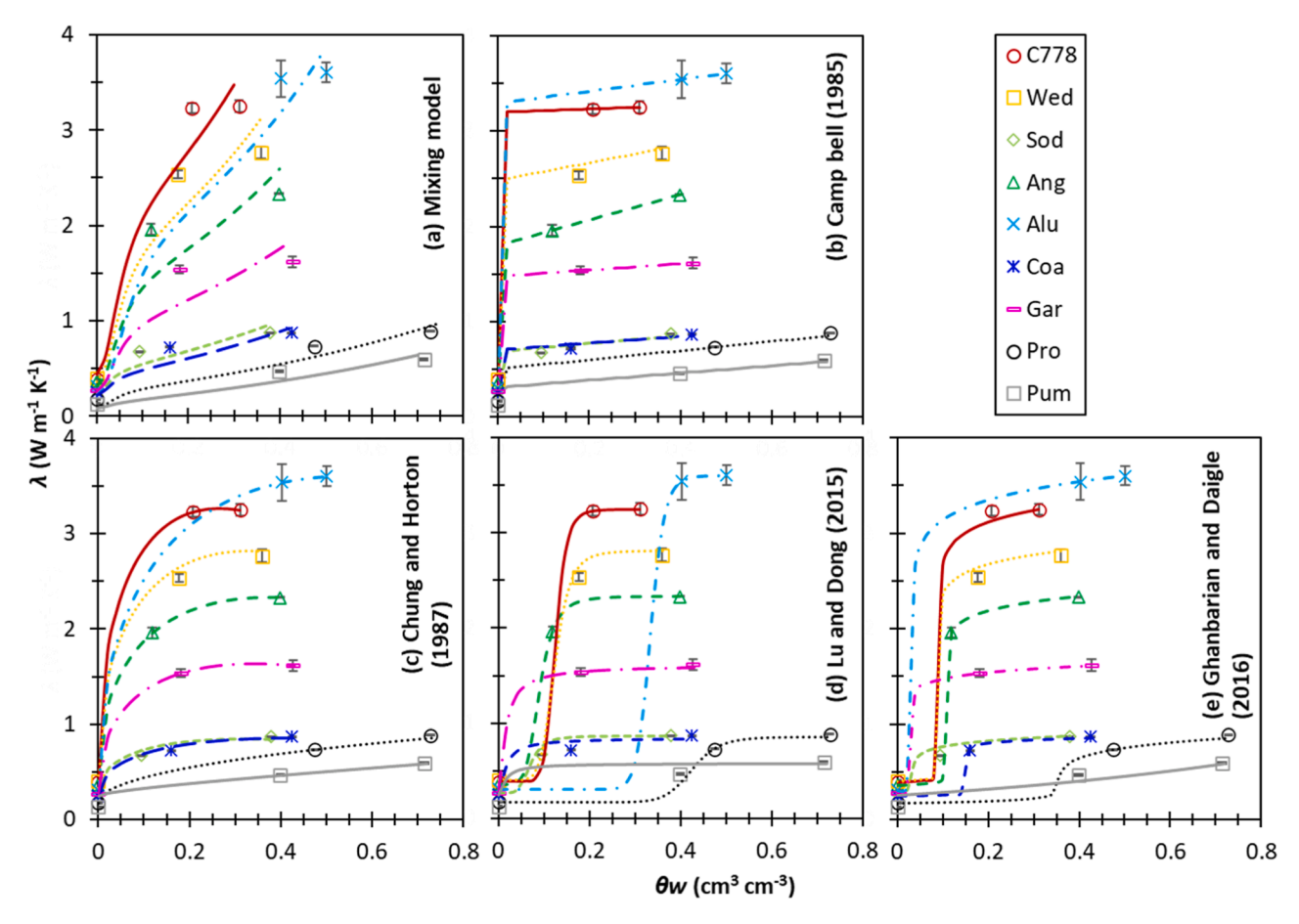


Fig. 4. The average λ functions determined by THPP (symbols) with the black bar representing the standard deviation. The fitted λ models, (a) the mixing model, (b) Campbell (1985) model, (c) Chung and Horton (1987) model, (d) Lu and Dong (2015) model and (e) Ghanbarian and Daigle (2016) model using the fitted parameter values shown in Table 4 are exhibited as lines.

fine sand (C778) (C778 ASTM graded silica sand, US Silica, Ottawa, IL, USA), Wedron sand (Wed) (Wedron silica Co., Wedron, IL), soda-lime glass beads (Sod) (GL0191B4/425–600, Mo-sci Specialty Products, L.L. C., Rolla, MO), (b) angular granular media: coarse angular sand (Ang) (2075, Industrial Quarts, Unimin Corp., Emmett, ID), aluminum oxide (Alu) (BLASTITE, Washington Mills, North Grafton, MA), coal slag (Coa) (BLACK BEAUTY Abrasives EXTRA FINE, Harsco Co., Mechanicsburg, PA), garnet (Gar) (#100/120 Grit, Blastline USA) and (c) aggregated media: Profile (Pro) (Profile Products LLC, Buffalo Grove, IL), pumice (Pum) (1/8" – 1/32" pumice, Scenic Hill Farm, Oregon, WA). Table 1 shows the physical properties of the selected granular materials. For additional details about the granular materials, see the product datasheet of each media.

The particle size distribution of each granular medium was measured by sieving samples for 15 min using a sieve shaker (CE Tyler RX-24, Combustion Engineering, New York, NY) and then weighing the material remaining on the series of sieves with opening sizes of 2.00, 1.70, 1.18, 1.00, 0.850, 0.710, 0.600, 0.500, 0.425, 0.355, 0.250, 0.212, 0.150, 0.125 and 0.053 mm based on the ASTM sieve size. The $\rho_{\rm S}$ of each granular medium were determined using the water displacement method (Dane and Topp, 2002).

3.3. Packing the granular media

A difficulty in using granular media is to establish and maintain a repeatable packing ρ_b . Packaging these media at various controlled θ_w values is further challenging. Packing dry particles eliminates the effects of wet media packing. Packing in water to saturate the media can lead to particle segregation and unintended layering of the media. We

employed the MSP method (Miura and Toki, 1982) to achieve a uniform dry granular medium $\rho_{\rm b}$ around the THPP. All samples were oven-dried at 105°C for at least 24 h and stored in sealed plastic bags to cool down and to begin measurements. A small diameter (0.25") funnel was positioned above a screen column as a hopper to maintain a uniform material flow. The stream of particles from the funnel was applied at a constant rate into a 220 mm long Lexan screen column (57 mm o.d., 51 mm i.d.) illustrated in Fig. 1a, containing five layers of steel wire screen (5 mm square openings), each layer 35 mm apart. The screen column was created by cutting 30 mm sections of the column and a 30 \times 30 mm square screen and sandwiching the heated screen (using a torch) between two column sections, effectively melting the wire into the column ends that also melted together. The completed screen column was connected to the top of the THPP column with a sleeve so that particles poured into the screen column would randomly scatter as they descended into the THPP column and effectively pummel the deposited material surface as a means of settling that surface to a consistent, repeatable density. We found this method avoids the unintended compaction around rods resulting from insertion into prepacked material. The dry $\rho_{\rm b}$ values in repeated packing trials of each material were virtually identical using this approach, as demonstrated in Table 1, with the largest standard deviation being just 0.6% of the mean dry ρ_b value for Profile (Pro). The screen column was removed, and the packed column was ready for the first heat pulse measurements.

After obtaining measurements on the dry media, the same packed material was saturated by injecting DI water into the media through the 1 cm diameter sintered stainless steel plate in the THPP base. The underside of the plate was glued to a barbed fitting and a small diameter tube that exited the lower pipe wall. The tube was useful for both adding

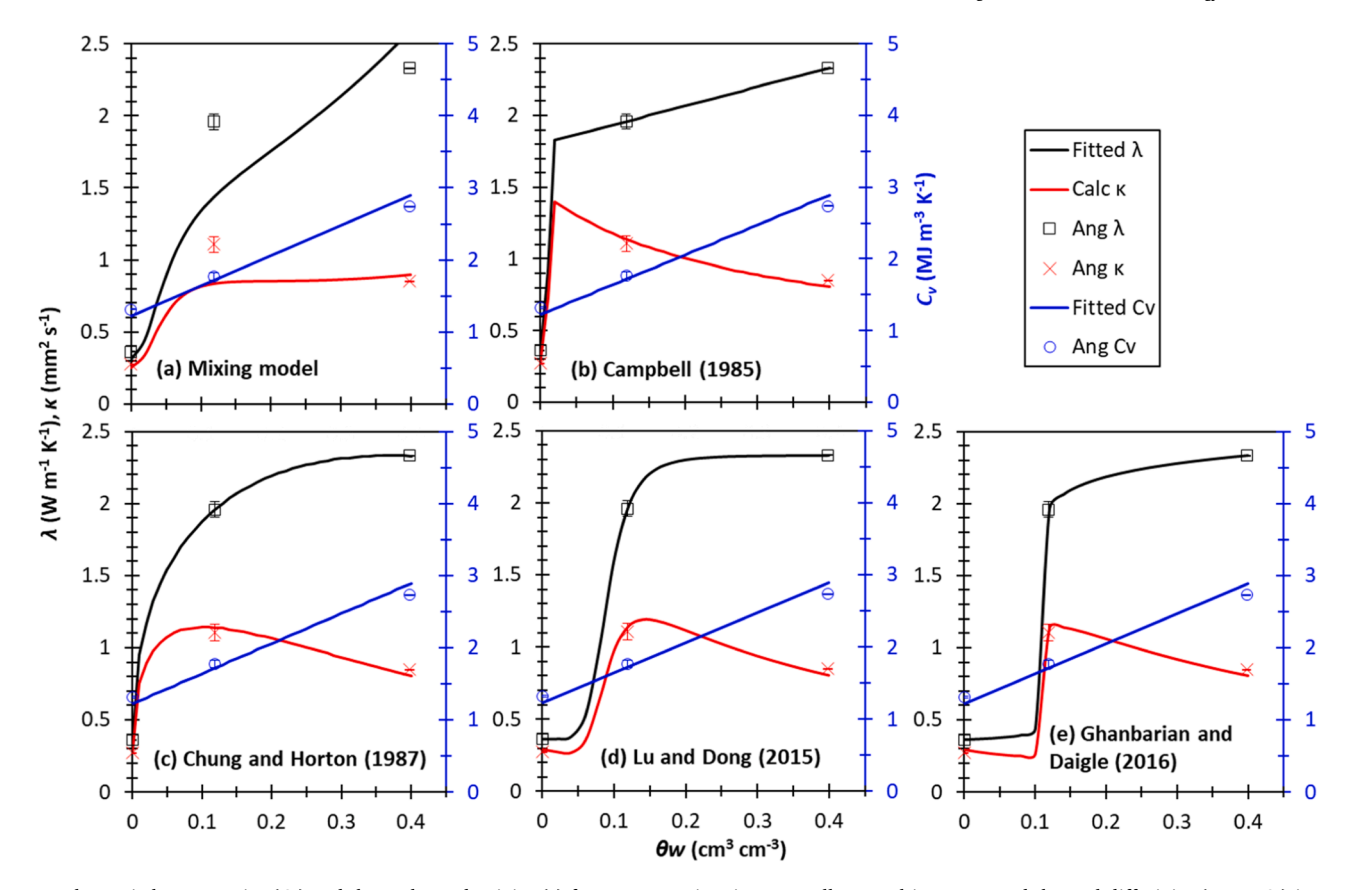


Fig. 5. Volumetric heat capacity (C_v) and thermal- conductivity (λ) from THPP estimations as well as resulting computed thermal diffusivity ($\kappa = \lambda/C_v$) in coarse angular sand (Ang) as shown assymbols. The blue line represents the optimized mixing model of C_v and each black lines represents λ models using (a) mixing model, (b) Campbell (1985), (c) Chung and Horton (1987), (d) Lu and Dong (2015) and (e) Ghanbarian and Daigle (2016) models. The red line illustrates the computed κ using the C_v mixing model and optimized λ model.

Table 3Diameters through which, respectively, 90%, 50% and 10% of the selected granular media passed. (% Fines is the mass of particles passing the 0.053 mm sieve).

Granular media	d_{90}	$d_{50} \ \mathrm{mm}$	d_{10}	Fines %
C778	0.500	0.425	0.355	0
Wed	0.400	0.250	0.150	2.7
Sod	0.600	0.500	0.425	0
Ang	1.18	0.850	0.600	0
Alu	0.212	0.150	0.125	0.3
Coa	0.600	0.400	0.355	0.1
Gar	0.212	0.150	0.125	1.2
Pro	0.710	0.600	0.425	0
Pum	2.00	1.70	1.00	

and removing water from a sample. The Lexan column was sealed at the top using an O-ring adorned plug with a vacuum line connector exiting the top of the plug. We put the THPP column under a vacuum during water filling to minimize air entrapment in the granular medium. The total porosity (= $1-\rho_{\rm b}/\rho_{\rm s}$) of each packing was computed from $\rho_{\rm b}$ and $\rho_{\rm s}$ and used to determine the amount of water to inject to saturate the packed pore volume. After obtaining water-saturated measurements of the thermal properties, we connected a laboratory vacuum line, which maintained a static suction of -5.9 m and removed free water from the sintered stainless steel plate (previous water inlet) with air. After 60 min of the de-watering process, thermal property values at the quasiequilibrium $\theta_{\rm w}$ (drained $\theta_{\rm w}$) were obtained. Water additions and removals from each sample were verified by measuring changes in total column mass with a balance. Following the drained $\theta_{\rm w}$ measurements,

the θ_w of the packed samples were determined using the oven-drying method (Dane and Topp, 2002). The granular media packing method described here provides 1) oven-dried-, 2) saturated- and 3) drained- θ_w determinations of thermal property values in each granular material.

3.4. Data processing of temperature rise data for thermal property determinations

Thermal property (λ and C_v) values were estimated using a MATLAB program to fit the ICPC model (Eqs. (1-3)) to the measured temperature rise with time data. The apparent rod spacing value (r_c) was based on measurements in agar-stabilized water reported by Naruke et al. (2021) as shown in Table 2. Naruke et al. (2021) also reported the r_c values calibrated in air-free ice, and air-free ice could equally serve as calibration material as agar-stabilized water. Table 2 lists THPP rod configurations and input values, including the calibrated r_c and volumetric heat capacity for stainless steel and epoxy used in the ICPC model. Thermal diffusivity, κ , (= λ / C_v), was obtained using the fitted values of λ and C_v . Estimated C_v and λ at various θ_w conditions were used to determine parameter values for selected models of C_v (Eq. (4)) and λ (Eqs. (5-15)) for a θ_w range from oven-dry to saturation.

4. Results and discussion

4.1. Granular media as reference standards

The particle size distribution of each testing media was characterized in Fig. 2 and Table 3 as the particle diameter (mm) through which x% of a test granular medium passed as well as the fine particle content, which passed through the 53 μ m sieve. In most cases, diameters were greater

Table 4 Average and standard deviation (Stdev) of estimated C_v and λ , calculated κ (= C_v / λ) in granular media at oven-dry, saturated- and drained- water content (θ_w) conditions using the THPP measurements.

Granular media	$\theta_{ m w}$	C_{v}		λ		$\kappa (= C_{\rm v} / \lambda)$	$\kappa (= C_{\rm v} / \lambda)$	
		Average	Stdev	Average	Stdev	Average	Stdev	
	${\rm cm^3~cm^{-3}}$	MJ m	$^{-3} K^{-1}$	W m	$^{1} \text{ K}^{-1}$	mm^2	s^{-1}	
C778	0	1.3	0.019	0.39	0.0036	0.29	0.0046	
	0.21	2.3	0.16	3.2	0.053	1.4	0.11	
	0.31	2.7	0.15	3.3	0.061	1.2	0.092	
Wed	0	1.4	0.046	0.40	0.014	0.28	0.0060	
	0.18	2.1	0.11	2.5	0.043	1.2	0.080	
	0.36	2.7	0.25	2.8	0.065	1.0	0.071	
Sod	0	1.5	0.072	0.27	0.015	0.18	0.004	
	0.095	1.7	0.024	0.68	0.0018	0.39	0.0056	
	0.38	2.8	0.0077	0.87	0.0022	0.32	0.00022	
Ang	0	1.3	0.011	0.36	0.0041	0.28	0.00093	
-	0.12	1.8	0.051	0.91	0.054	1.1	0.057	
	0.40	2.7	0.0016	2.3	0.0022	0.85	0.00030	
Alu	0	1.5	0.061	0.31	0.014	0.20	0.0011	
	0.40	3.2	0.16	3.5	0.19	1.1	0.11	
	0.50	3.5	0.20	3.6	0.10	1.0	0.087	
Coa	0	1.3	0.034	0.25	0.0062	0.20	0.0067	
	0.16	2.0	0.067	0.41	0.0075	0.36	0.0082	
	0.43	2.9	0.011	0.87	0.0043	0.31	0.0023	
Gar	0	1.6	0.080	0.28	0.018	0.17	0.0038	
	0.18	2.5	0.15	1.5	0.042	0.61	0.025	
	0.43	3.0	0.17	1.6	0.059	0.55	0.029	
Pro	0	0.63	0.013	0.17	0.0026	0.27	0.0094	
	0.48	2.6	0.012	0.73	0.0035	0.29	0.0025	
	0.73	3.5	0.035	0.89	0.0042	0.25	0.0037	
Pum	0	0.52	0.015	0.13	0.0022	0.25	0.011	
	0.40	2.0	0.096	0.47	0.0093	0.23	0.0066	
	0.71	3.1	0.033	0.59	0.0090	0.19	0.0024	

Table 5Estimated thermal parameters for thermal property functions.

	C778	Wed	Sod	Ang	Alu	Coa	Gar	Pro	Pum
				$C_{\rm v}$ — mixing	model				
$c_{\rm s}$	761	820	846	761	743	739	685	781	652
$(J kg^{-1} K^{-1})$									
				λ – mixing r					
$\lambda_{\rm s}$ (W m ⁻¹ K ⁻¹)	7.1	6.3	1.2	5.4	27	1.2	3.7	2.3	0.83
(W m - K -)				λ – Campbell (19	195) model				
Α	3.2	2.5	0.69	1.8	3.3	0.71	1.5	0.51	0.31
В	0.17	0.91	0.41	1.3	0.62	0.35	0.33	0.48	0.31
C	83	83	83	83	83	83	83	83	83
D	0.39	0.40	0.27	0.36	0.31	0.25	0.28	0.17	0.25
E	4	4	4	4	4	4	4	4	4
			λ –	Chung and Horton	n (1987) model				
b_1	0.39	0.40	0.27	0.36	0.31	0.25	0.28	0.17	0.25
b_2	-11	-7.3	-1.8	-5.3	-6.0	-1.4	-4.0	-0.094	0.26
b_3	11	8.4	2.1	6.5	8.9	1.8	4.7	0.88	0.18
				. – Lu and Dong (2					
$\lambda_{ m dry} \ ({ m W~m^{-1}~K^{-1}})$	0.39	0.40	0.27	0.36	0.31	0.25	0.28	0.17	0.25
$\lambda_{\rm sat}$ (W m ⁻¹ K ⁻¹)	3.2	2.8	0.87	2.3	3.6	0.85	1.6	0.85	0.58
$\theta_{ m wf}$	0.12	0.12	0.066	0.087	0.33	0.010	0.010	0.42	0.010
$(cm^3 cm^{-3})$									
m	11	7.9	5.4	6.0	22	2.0	2.0	14	2.0
1.	0.39	0.40	0.27	nanbarian and Dai 0.36	0.31	0.25	0.28	0.17	0.25
$\lambda_{ m dry} \ ({ m W~m^{-1}~K^{-1}})$	0.39	0.40	0.27	0.30	0.51	0.23	0.28	0.17	0.23
λ_{sat} (W m ⁻¹ K ⁻¹)	3.2	2.8	0.87	2.3	3.6	0.85	1.6	0.85	0.58
θ_{wc}	0.092	0.089	0.062	0.11	0.033	0.15	0.026	0.46	0
$(\text{cm}^3 \text{ cm}^{-3})$		5.303							
t_{s}	0.059	0.057	0.063	0.055	0.071	0.038	0.053	0.053	2.0

than 53 μ m, correlating with a sandy texture. The finest medium was aluminum oxide (Alu) and garnet (Gar), and the coarsest was pumice (Pum). Most of the particles in pumice (Pum) were larger than 1 mm, however, the sieving process broke particles down into smaller fractions

in some of the weaker aggregated media, making particle diameter determination challenging. Soda-lime glass beads (Sod) showed a very narrow distribution, while Wedron sand (Wed) exhibited a relatively wide distribution. In addition to Wedron sand (Wed), both aluminum

Table 6RMSE of thermal property functions in various testing media.

C778	Wed	Sod	Ang	Alu	Coa	Gar	Pro	Pum
			C _v (M.	$J m^{-3} K^{-1}$) – mixing	model			
0.13	0.18	0.17	0.11	0.15	0.14	0.29	0.12	0.19
			λ (W	$m^{-1} K^{-1}$) – mixing m	nodel			
0.30	0.36	0.13	0.34	0.29	0.095	0.25	0.10	0.12
			λ (W m ⁻¹	K^{-1}) – Campbell (19	85) model			
0.043	0.057	0.032	0.029	0.12	0.040	0.039	0.022	0.015
			$\lambda \ (W \ m^{-1} \ K^{-1})$	- Chung and Horton	(1987) model			
0.043	0.057	0.022	0.029	0.12	0.040	0.039	0.022	0.015
			λ (W m ⁻¹ K	$^{-1}$) – Lu and Dong (2	2015) model			
0.043	0.057	0.0092	0.029	0.12	0.052	0.043	0.022	0.066
			λ (W m ⁻¹ K ⁻¹) –	Ghanbarian and Dai	gle (2016) model			
0.073	0.057	0.0092	0.029	0.14	0.040	0.039	0.022	0.031

oxide (Alu) and garnet (Gar) exhibited similar effective particle size distributions. Coarse angular sand (Ang), Wedron sand (Wed), and fine silica sand (C778) had high quartz content (>90%), and these three materials presented similar particle size distributions. Each granular medium was carefully packed using the MSP method, which worked well for most granular media. However, finer particles such as aluminum oxide (Alu) and garnet (Gar) passed through the screens and were less effectively scattered, leading to a cone-shaped surface rather than a flat surface during packing. A smaller mesh opening size may increase particle scattering for finer materials and be used as additional standard granular media.

4.2. Thermal property estimation in granular media

4.2.1. Thermal property determination using the air-MSP method

As shown in Table 1, the air-MSP method resulted in consistent ρ_b values for the different test media. Pumice (Pum) showed a relatively larger standard deviation of ρ_b value of 1.17 kg m $^{-3}$ with a mean ρ_b value of 488 kg m $^{-3}$ and we triplicated pumice trial to provide the likelihood of errors in estimated thermal property values. Thermal property (λ , C_v and κ) estimations using THPP measurements with two thermistor rods, T_a and T_b , with a triplicated air-MSP trial in oven-dried pumice showed small standard deviations of 1.8×10^{-3} W m $^{-1}$ K^{-1} in λ , 1.6×10^{-2} MJ m $^{-3}$ K $^{-1}$ in C_v and 1.0×10^{-2} mm 2 s $^{-1}$ in κ , and each standard deviation value had less than 1, 3 and 4% in each of mean thermal properties (data not shown). Therefore, THPP measurements combined with the air-MSP method provided reproducible thermal property estimations in granular media.

4.2.2. Thermal property estimation at different water contents

Table 4 lists the averages and standard deviations (Stdev) of thermal property values estimated by fitting the ICPC model to triplicated measurements of temperature rise with time in both thermistor-rods, T_a and T_b therefore six data sets at oven-dry, saturated- and drained- θ_w conditions. We combined thermal property results from T_a and T_b to provide a range of errors in estimating each thermal property value. Estimated thermal property values exhibited ranges in C_v of 0.52 to 3.5 MJ m⁻³ K⁻¹, in λ of 0.13 to 3.6 W m⁻¹ K⁻¹, and in κ of 0.17 to 1.4 mm² s^{-1} . Most of the media showed minimal standard deviations at the ovendry condition and larger standard deviations at drained- and saturation- $\theta_{\rm w}$ conditions. The larger standard deviations at drained- and saturation- $\theta_{\rm w}$ conditions in fine-textured granular media, such as fine sand (C778), Wedron sand (Wed), aluminum oxide (Alu) and garnet (Gar), might be due in part to trapped air between particles creating non-homogeneous conditions. The saturated $\theta_{\rm w}$ value in these media during the infusion process was smaller than the porosity value. Dane and Hopmans (2002) reported that $\theta_{\rm w}$ value at saturation during the wetting process is commonly about 85% of saturation $\theta_{\rm W}$ at the complete saturation condition. While the dry and saturated media are considered to possess uniform properties and resulting repeatable thermal properties, the partially wetted media also showed small deviations in their thermal

property determinations as a result, indicating that the water distribution in the column at the drained θ_w was also relatively uniform.

Thermal properties (C_v , λ and κ) at our three target θ_w conditions represented different combinations of the three solid, water and air phases within the testing media. For the oven-dry condition, thermal properties depended only on the solid and air phases, while all three phases affected thermal properties for saturated- and for drainedconditions. The C_v measurements at the three different θ_w conditions presented increasing $C_{\rm v}$ as $\theta_{\rm w}$ increased. The two aggregated media (Proand Pum) had oven-dried C_{ν} values at around half of the rest of the granular media tested, due to the lower ρ_b values (higher air content). Oven-dry λ measurements in Table 4 exhibited a narrow range from 0.13 to 0.40 W m⁻¹ K⁻¹, while saturated λ had a much larger range from 0.61 to 3.71 W m^{-1} K⁻¹. The three different quartz sands (C778, Wed and Ang) exhibited the highest oven-dry λ values ranging between 0.36 and 0.40 W m⁻¹ K⁻¹, while the two aggregated media (Pro-and Pum) exhibited the lowest oven-dry λ values of 0.17 and 0.13 W m⁻¹ K⁻¹, respectively, due to the lower ρ_b values. Although particle shape (e.g., spherical and ellipsoidal) and packing method (e.g., random packing vs. vibration) affect ρ_b and contact between particle to particle and particle to different phase(s) (Dai et al., 2019), our thermal property measurements using THPP did not show substantial difference among three different categories (spherical, angular and aggregated) except for aggregated- and non-aggregated- media.

Some of these test media exhibited a rapid increase in λ when $\theta_{\rm W}$ increased from oven-dry to the drained condition, followed by a more moderate increase in λ after θ_w increased between the drained condition and saturation (e.g., Ang, C778, Wed and Gar). Other media exhibited a gradual monotonic increase in λ for the entire $\theta_{\rm w}$ range (e.g., Sod, Coa, Pro, and Pum). The rapid increase of λ in the relatively dry condition was caused by growing pendular rings (also called capillary bridges) (de Bisschop and Rigole, 1982; Rose, 1958) which increased the contact area, and thus, the heat transfer between solid particles. This occurred until the effect of water became insignificant when $\theta_{\rm w}$ was high. Among the three λ functions of quartz sand (Ang, C778 and Wed), the fine sand (C778) with the highest ρ_b (1829 kg m⁻³) had the largest λ function, while Ang with the lowest ρ_b (1607 kg m⁻³) presented the lowest values of thermal conductivity. Soda-line glass beads (Sod) and coal slag (Coa) had similar λ functions, explained by similar quartz content and ρ_b . Aggregated media such as Profile (Pro) and pumice (Pum) had relatively small λ across a wide range of $\theta_{\rm w}$. Because both Profile and pumice had internal aggregation, intra-aggregate entrapped air had a large effect on λ , while water mainly filled most of the external aggregate pores and internal aggregate pores were filled mostly with air. Thermal diffusivity (κ) measurements showed the largest κ at the drained $\theta_{\rm W}$ in all media except for pumice (Pum). Since κ was calculated as $\kappa = C_V / \lambda$, moderate increases in λ for $\theta_{\rm W}$ beyond the drained condition to saturation led to decreasing κ toward the saturated condition.

These coarse granular media presented distinct wetting/drying fronts when water was pushed into or drained from the column. The ICPC model assumed a uniform distribution of materials including water

and solid phases, therefore, our thermal property measurements were limited at the three target $\theta_{\rm w}$ conditions for our vertical rod orientation. The vertical orientation was also advantageous to provide repeatable bulk packing density in the granular media using air-MSP method.

4.3. Thermal property models

4.3.1. Volumetric heat capacity

In Fig. 3, the average- and standard deviation values of C_v versus θ_w for the eight granular media listed in Table 4 were plotted as circle symbols and black solid bars. The optimized mixing model of C_v (Eq. (4)) using the fitted parameter, c_s listed in Table 5

for each media is exhibited as the solid line. Since the fitted parameter was only c_s , which determined the offset value of the C_V function, the slope of all lines was determined by θ_w multiplied by the volumetric heat capacity of water ($C_w = \rho_w \times c_w = 4.18$ MJ m⁻³ K⁻¹). The C_V function of aggregated media, Profile and pumice as shown as black- and gray- circles showed lower trends than for other media due to lower ρ_b values of 693 and 488 kg m⁻³, respectively.

Estimated c_s in testing media (Table 5 showed that soda-lime glass beads (Sod) and pumice (Pum) had the highest- and lowest- c_s of 846 and 652 J kg⁻¹ K⁻¹, respectively. The average estimated c_s values for three different quartz sands (Ang, C778, Wed) was 781 J kg⁻¹ K⁻¹ with highest- and lowest- c_s values of 820 and 761 J kg⁻¹ K⁻¹, in Wedron sand (Wed) and C778, respectively. Reported c_s values in soda-lime glass beads (Ham and Benson, 2004; Tarara and Ham, 1997) and quartz sand (Bristow et al., 1994) were 794 and 802 J kg⁻¹ K⁻¹, respectively. Although our estimated c_s value in soda-lime glass beads (Sod) was greater than the reported values, our c_s in quartz sands (Ang. C778, Wed) followed literature values. Thermal conductivity functions using the mixing model (Eqs. (5-8)), Campbell (1985) model (Eqs. (9 and 10)), Chung and Horton (1987) model (Eq. (11)), Lu and Dong (2015) model (Eq. (12)) and Ghanbarian and Daigle (2016) model (Eqs. (13-15)) were compared with THPP determined λ values in Fig. 4a–4e, respectively. Square symbols and the black bars represent the average and the standard deviation of λ estimates in Table 4, respectively. Fitted λ models are shown as lines in Fig. 4a-4e, and optimized model parameters are presented in Table 5.

With only three λ measurement points at three different $\theta_{\rm w}$ conditions (i.e., oven-dry, saturated and drained) in coarse granular media, it was challenging to predict the transition point in the existing λ functions because of the lack of measurements at additional low $\theta_{\rm W}$. The model fitting could be improved if additional measurements of λ at low θ_w values were available. In Fig. 4a, the mixing model agreed well with λ at the oven-dry condition in all media, however, the mixing model showed an underestimation of λ values at the drained θ_w while overestimating λ values at saturation. The Campbell (1985) model exhibited an earlier λ transition point at the $\theta_{\rm w}$ value of around 0.04 cm³ cm⁻³ because the parameter, C, in the model was the only parameter to determine the transition point, and we assumed C = 83 due to the coarse texture of our media (see Table 5) as discussed earlier. Parameters presented in Table 5 were used to inform the empirical Campbell (1985) model shown in Fig. 4b. The empirical Chung and Horton (1987) model showed a smooth increase in λ at lower- $\theta_{\rm w}$ ranges, unlike the Campbell (1985) model. The Chung and Horton (1987) model parameters, b1, b2 and b3 were presented in Table 5, and b_1 which determined the λ_{dry} , was the same value in all media as parameter *D* in the Campbell (1985) model. The conceptual Lu and Dong (2015) model created a sigmoidal function in most media except for coal slag (Coa), garnet (Gar) and pumice (Pum). The model used the parameters of λ_{dry} and λ_{sat} as shown in Table 5 to set a lower- and higher- end of the model with curve shape parameters θ_f and m, therefore the Lu and Dong (2015) model exhibited a plateau at higher $\theta_{\rm W}$ values. Lu and Dong (2015) provided the relationship between water retention characteristics and their curve shape parameters θ_f , which might increase the accuracy of the model prediction if these water retention parameters were available. For example,

Profile has almost 1:1 fraction of dual porosity structure described as inter-aggregate (0.37) and intra-aggregate pores (0.37) where water held in macro pores drain at the matric potential around –25 cm (Heinse et al., 2007). The θ_f value of Profile (Pro) in the Lu and Dong (2015) model was 0.42 cm³ cm⁻³, which was close to the threshold θ_w (0.37 cm³ cm⁻³) of the dual porosity structure. The theoretical Ghanbarian and Daigle (2016) model produced a variety of $\lambda(\theta_w)$ curves where the curve exhibited a monotonic increase in Pum (gray) due to a larger t_s value (t_s = 2). The Ghanbarian and Daigle (2016) model also showed a curve similar to a step-function when t_s was close to 0, where λ showed a substantial increase at $\theta_w = \theta_{cw}$ as shown in Table 5.

Unlike the sigmoid function by the Lu and Dong (2015) model, the Ghanbarian and Daigle (2016) still exhibited a monotonic increase after λ showed a substantial increase ($\theta_{\rm w} > \theta_{\rm wc}$) in some media (e.g., C778). The Ghanbarian and Daigle (2016) model in Profile (Pro) also showed a λ curve which was similar to the λ curve using the Lu and Dong (2015) model. Although the $\theta_{\rm wc}$ optimization in Profile (Pro) showed a potential to relate the media's water retention characters and the $\theta_{\rm wc}$ value, the $\theta_{\rm wc}$ values optimized for finer granular media (e.g., aluminum oxide (Alu) and garnet (Gar)) could be poorly described due to our limited data. Since both aluminum oxide (Alu) and garnet (Gar) had finer particle sizes, the expected $\theta_{\rm wc}$ values may be much greater than the optimized $\theta_{\rm wc}$ values.

The accuracy of $C_{\rm v}$ and λ models in test media was evaluated by calculating RMSE (Eq. (15)), and values are presented in Table 6. The $C_{\rm v}$ mixing model showed consistent RMSE values with a minimum RMSE of 0.11 MJ m $^{-3}$ K $^{-1}$ in coarse angular sand (Ang) and a maximum RMSE of 0.29 MJ m $^{-3}$ K $^{-1}$ in garnet (Gar). Garnet (Gar) exhibited relatively large fluctuations in THPP $C_{\rm v}$ determinations, which increased RMSE in the $C_{\rm v}$ model fitting. Four of five λ models (mixing model was an exception) showed almost the same RMSE value in each test media. The λ mixing model RMSE values were more than double the values of the other media, and therefore we do not recommend the application of the mixing model of λ unless the model is well optimized with λ measurements at lower $\theta_{\rm w}$ conditions.

Finally, Fig. 5 presents the THPP-determined C_{ν} and λ values and the resulting values of κ ($\kappa = \lambda/C_v$) for coarse angular sand (Ang) at the ovendried-, saturated- and drained- $\theta_{\rm W}$ conditions. Fig. 5a-5e also includes the optimized mixing model results for C_{ν} as blue lines, while each black curve represents the optimized λ model using (a) mixing model, (b) Campbell (1985) model, (c) Chung and Horton (1987) model, (d) Lu and Dong (2015) model and (e) Ghanbarian and Daigle (2016) model, respectively. The red curves represent κ values computed from the optimized models of C_v and λ as $(\kappa = \lambda/C_v)$. The λ model selection directly affects κ values. For example, the computed κ using the mixing model of C_v and λ showed underestimations in the drained water values due to the underestimation of λ with the mixing model (Fig. 5a). Thermal property values at the water content lower than the drained water content values are especially important for simulating the transport of water, gas and energy under dry conditions, therefore selecting the most representative thermal conductivity model is important for accurate representation of κ values.

5. Conclusions

This study presented concepts for standardized estimated thermal properties of nine commercially available coarse granular media at different volumetric water content ($\theta_{\rm w}$) conditions using a Three-rod Heat Pulse Probe (THPP). Commercially available granular media included spherical-, angular- and aggregated- materials. We reported particle size distribution for each media, and the particle density ($\rho_{\rm s}$) values ranged from 1718 to 4019 kg m⁻³. The Multiple Sieving Pluviation (MSP) method provided highly repeatable packing represented by bulk density ($\rho_{\rm b}$) values ranging from 488 to 2205 kg m⁻³ in these granular materials within 0.6% of standard deviation. The Identical Cylindrical Perfect Conductors (ICPC) model was applied to the THPP

temperature rise measurements to determine the thermal property values of each granular material at three different θ_w values. Oven-dry granular media exhibited thermal property values ranging from 0.52 to 1.6 MJ m⁻³ K⁻¹ for volumetric heat capacity (C_v), 0.13 to 0.4 W m⁻¹ K^{-1} for thermal conductivity (λ) and 0.17 to 0.29 mm² s⁻¹ for thermal diffusivity (κ) , and the thermal property values of saturated media ranged from 2.7 to 3.5 MJ m⁻³ K⁻¹ for $C_{\rm v}$, 0.59 to 3.6 W m⁻¹ K⁻¹ for λ and 0.19 to 1.2 mm² s ⁻¹ for κ . Estimated thermal properties ($C_{\rm v}$, λ and κ) with a wide range of θ_w (i.e., from oven-dry to saturation) at highly repeatable ρ_b in various granular media improve thermal property sensor development and could also serve as additional calibration media. We also provided optimized parameters for existing thermal property (C_v and λ) models based on our granular media measurements. The C_v mixing model well described the THPP-determined C_v values as a linear model in all media. The λ mixing model showed more than double RMSE values in all media compared to the other four models including two empirical λ models by Campbell (1985) and Chung and Horton (1987), the conceptual λ model developed by Lu and Dong (2015), as well as the theoretical model developed by Ghanbarian and Daigle (2016). These four models showed more flexibility to characterize THPP-determined λ values compared to the λ mixing model, however, insufficient λ data at low-range θ_w conditions leave some uncertainty in the optimal shape of the λ function. As mentioned, a limitation of this approach is the lack of THPP measurements at low-range $\theta_{\rm W}$ conditions and additional information (e.g., soil hydraulic properties) of testing media could also improve the parameter optimization for λ models. (Figs. 3 and 4, Table 3)

Declaration of Competing Interest

The authors declare that they have no known competing financial interests or personal relationships that could have appeared to influence the work reported in this paper.

Data availability

Data will be made available on request.

Acknowledgments

This research was supported by the Utah Agricultural Experiment Station, Utah State University, USDA-NIFA Multi-State Project 4188, and approved as journal paper number 9561.

References

- ASTM Committee p-18 on Soil and Rock, 2006. Standard Test Methods For Minimum Index Density and Unit Weight of Soils and Calculation of Relative Density. ASTM International, Philadelphia, Pa.
- ASTM International. Subcommittee D18. 12 on Rock Mechanic, 2008. Standard test method for determination of thermal conductivity of soil and soft rock by thermal needle probe procedure.
- Bilskie, J.R., Horton, R., Bristow, K.L., 1998. Test of a dual-probe heat-pulse method for determining thermal properties of porous materials1. Soil sci. 163, 346–355.
- Bittelli, M., Campbell, G.S., Tomei, F., 2015. Soil physics with python: transport in the soil–plant–atmosphere system oxford scholarship.
- Bristow, K.L., 1998. Measurement of thermal properties and water content of unsaturated sandy soil using dual-probe heat-pulse probes. Agric. For. Meteorol. 89, 75–84. https://doi.org/10.1016/S0168-1923(97)00065-8.
- Bristow, K.L., Kluitenberg, G.J., Horton, R., 1994. Measurement of soil thermal properties with a dual-probe heat-pulse technique. Soil Sci. Soc. Am. J. 58, 1288–1294. https://doi.org/10.2136/sssaj1994.03615995005800050002x.
- Campbell, G.S., 1985. Soil Temperature and Heat Flow, in: Soil Physics With Basic. Elsevier, pp. 26–39. https://doi.org/10.1016/s0166-2481(08)70134-x.
- Campbell, G.S., Calissendorff, C., Williams, J.H., 1991. Probe for measuring soil specific heat using a heat-pulse method. Soil Sci. Soc. Am. J. 55, 291–293. https://doi.org/10.2136/sssai1991.03615995005500010052x.
- Campbell, G.S., Jungbauer, J.D., Bidlake, W.R., Hungerford, R.D., 1994. Predicting the effect of temperature on soil thermal conductivity. Soil Sci. 158, 307–313. https:// doi.org/10.1097/00010694-199411000-00001.

- Chung, S., Horton, R., 1987. Soil heat and water flow with a partial surface mulch. Water Resour Res. 23, 2175–2186. https://doi.org/10.1029/WR023i012p02175.
- Cobos, D.R., Baker, J.M., 2003. Situ Measurement of Soil Heat Flux with the Gradient Method. Vadose Zone J. 2, 589–594. https://doi.org/10.2113/2.4.589.
- Dai, W., Hanaor, D., Gan, Y., 2019. The effects of packing structure on the effective thermal conductivity of granular media: a grain scale investigation. Int. J. Thermal Sci. 142, 266–279. https://doi.org/10.1016/J.IJTHERMALSCI.2019.04.028.
- Dane, J.H., Hopmans, J.W., 2002. Hanging water column. In: Dane, J.H., Topp, G.C. (Eds.), Method of Soil Analysis: Part 4 Physical Methods. Soil Science Society of America, pp. 680–683.
- Dane, J.H., Topp, G.C., 2002. Methods of Soil Analysis, SSSA Book Series. Soil Science Society of America, Madison, WI, USA. https://doi.org/10.2136/sssabookser5.4.
- de Bisschop, F.R.E., Rigole, W.J.L., 1982. A physical model for liquid capillary bridges between adsorptive solid spheres: the nodoid of plateau. J. Colloid Interface Sci. 88, 117–128. https://doi.org/10.1016/0021-9797(82)90161-8.
- de Vries, D.A., 1963a. Thermal properties of soils. In: van Wijk, W.R. (Ed.), Physics of Plant Environment. North-Holland Publishing Company, Amsterdam, pp. 210–235.
- de Vries, D.A., 1963b. CHAPTER 2 The Physics of Plant Environments. In: Evans, L.T. (Ed.), Environmental Control of Plant Growth. Academic Press, pp. 5–22.
- Dong, Y., McCartney, J.S., Lu, N., 2015. Critical review of thermal conductivity models for unsaturated soils. Geotech. Geolog. Engin. 33, 207–221. https://doi.org/ 10.1007/s10706-015-9843-2.
- Farouki, O.T., 1981. Thermal properties of soils.
- Gan, J., Yu, A., 2020. DEM study on the packing density and randomness for packing of ellipsoids. Powder Technol. 361, 424–434. https://doi.org/10.1016/J. POWTEC.2019.07.012.
- Ghanbarian, B., Daigle, H., 2016. Thermal conductivity in porous media: percolation-based effective-medium approximation. Water Resour. Res. 52, 295–314. https://doi.org/10.1002/2015WR017236.
- Guaraglia, D.O., Pousa, J.L., 1999. An electrical model of heat flow in soil. Soil Sci. Soc. Am. J. 63, 457–463. https://doi.org/10.2136/ SSSAJ1999.03615995006300030006X.
- Ham, J.M., Benson, E.J., 2004. On the construction and calibration of dual-probe heat capacity sensors. Soil Sci. Soc. Am. J. 68, 1185–1190. https://doi.org/10.2136/ sssaj2004.1185.
- He, H., Dyck, M.F., Horton, R., Ren, T., Bristow, K.L., Lv, J., Si, B., 2018. Development and application of the heat pulse method for soil physical measurements. Rev. Geophys. 56, 567–620. https://doi.org/10.1029/2017RG000584.
- He, H., Zhao, Y., Dyck, M.F., Si, B., Jin, H., Lv, J., Wang, J., 2017. A modified normalized model for predicting effective soil thermal conductivity. Acta Geotech. 12, 1281–1300. https://doi.org/10.1007/S11440-017-0563-Z/FIGURES/5.
- Heinse, R., Jones, S.B., Steinberg, S.L., Tuller, M., Or, D., 2007. Measurements and modeling of variable gravity effects on water distribution and flow in unsaturated porous media. Vadose Zone J. 6, 713–724. https://doi.org/10.2136/VZJ2006.0105.
- Heitman, J.L., Horton, R., Sauer, T.J., DeSutter, T.M., 2008. Sensible Heat Observations Reveal Soil-Water Evaporation Dynamics. J. Hydrometeorol. 9, 165–171. https://doi.org/10.1175/2007JHM963.1.
- Hopmans, J.W., Šimunek, J., Bristow, K.L., 2002. Indirect estimation of soil thermal properties and water flux using heat pulse probe measurements: geometry and dispersion effects. Water Resour. Res. 38 https://doi.org/10.1029/2000wr000071, 7-1-7-14
- Kluitenberg, G.J., Philip, J.R., 1999. Dual thermal probes near plane interfaces. Soil Sci. Soc. Am. J. 63, 1585–1591. https://doi.org/10.2136/SSSAJ1999.6361585X.
- Knight, J.H., Kluitenberg, G.J., Kamai, T., Hopmans, J.W., 2012. Semianalytical solution for dual-probe heat-pulse applications that accounts for probe radius and heat capacity. Vadose Zone J. 11 https://doi.org/10.2136/vzj2011.0112.
- Kodicherla, S.P.K., Gong, G., Fan, L., Moy, C.K.S., He, J., 2018. Effects of preparation methods on inherent fabric anisotropy and packing density of reconstituted sand. htt p://www.editorialmanager.com/cogenteng 5, 1–14. https://doi.org/10.1080/ 23311916.2018.1533363.
- Liu, G., Wen, M., Chang, X., Ren, T., Horton, R., 2013. A self-calibrated dual probe heat pulse sensor for in situ calibrating the probe spacing. Soil Sci. Soc. Am. J. 77, 417–421. https://doi.org/10.2136/SSSAJ2012.0434N.
- Lu, N., Dong, Y., 2015. Closed-Form Equation for Thermal Conductivity of Unsaturated Soils at Room Temperature. J. Geotech. Geoenviron. Engin. 141, 04015016 https:// doi.org/10.1061/(ASCE)GT.1943-5606.0001295.
- Lu, S., Lu, Y., Peng, W., Ju, Z., Ren, T., 2019. A generalized relationship between thermal conductivity and matric suction of soils. Geoderma 337, 491–497. https://doi.org/ 10.1016/j.geoderma.2018.09.057.
- Lu, Y., Lu, S., Horton, R., Ren, T., 2014. An empirical model for estimating soil thermal conductivity from texture, water content, and bulk density. Soil Sci. Soc. Am. J. 78, 1859–1868. https://doi.org/10.2136/sssaj2014.05.0218.
- Miura, S., Toki, S., 1982. A sample preparation method and its effect on static and cyclic deformation-strength properties of sand. Soils Found. 22, 61–77. https://doi.org/ 10.3208/SANDF1972.22.61.
- Naruke, C., Sheng, W., Zhou, R., Jones, S.B., 2021. Standardizing Heat Pulse Probe measurements for thermal property determination using ice and water. Agric. For. Meteorol. 308–309, 108610 https://doi.org/10.1016/J.AGRFORMET.2021.108610.
- Noborio, K., McInnes, K.J., Heilman, J.L., 1996. Measurements of soil water content, heat capacity, and thermal conductivity with a single TDR probe. Soil Sci. 161, 22–28. https://doi.org/10.1097/00010694-199601000-00004.
- Ochsner, T.E., Sauer, T.J., Horton, R., 2007. Soil heat storage measurements in energy balance studies. Agron. J 99, 311–319. https://doi.org/10.2134/agronj2005.01038
- Peng, W., Lu, Y., Ren, T., Horton, R., 2021. Application of infinite line source and cylindrical-perfect-conductors theories to heat pulse measurements with large sensors. Soil Sci. Soc. Am. J. 85, 1050–1059. https://doi.org/10.1002/SAJ2.20250.

- Peng, W., Lu, Y., Xie, X., Ren, T., Horton, R., 2019. An improved thermo-TDR technique for monitoring soil thermal properties, water content. Bulk Dens. Porosity. Vadose Zone J. 18, 1–9. https://doi.org/10.2136/vzj2019.03.0026.
- Rose, W., 1958. Volumes and surface areas of pendular rings. J. Appl. Phys. 29, 687. https://doi.org/10.1063/1.1723251.
- Sadeghi, M., Ghanbarian, B., Horton, R., 2018. Derivation of an explicit form of the percolation-based effective-medium approximation for thermal conductivity of partially saturated soils. Water Resour. Res. 54, 1389–1399. https://doi.org/ 10.1002/2017WR021714.
- Shi, J., Haegeman, W., Mascini, A., Cnudde, V., 2021. X-ray analysis on the effect of sample preparation on the microstructure of calcareous sands. Marine Georesour. Geotechnol. 39, 302–311. https://doi.org/10.1080/1064119X.2019.1698680.
- Tabaroei, A., Abrishami, S., Hosseininia, E.S., 2017. Comparison between Two Different Pluviation Setups of Sand Specimens. J. Mater. in Civil Engin. 29, 04017157 https://doi.org/10.1061/(ASCE)MT.1943-5533.0001985.
- Tarara, J.M., Ham, J.M., 1997. Measuring soil water content in the laboratory and field with dual-probe heat-capacity sensors. Agron J. 89, 535–542. https://doi.org/ 10.2134/agronj1997.00021962008900040001x.

- Tian, Z., Lu, Y., Horton, R., Ren, T., 2016. A simplified de Vries-based model to estimate thermal conductivity of unfrozen and frozen soil. Eur. J. Soil Sci. 67, 564–572. https://doi.org/10.1111/EJSS.12366.
- van Genuchten, M.Th., 1980. A closed-form equation for predicting the hydraulic conductivity of unsaturated soils. Soil Sci. Soc. Am. J. 44, 892–898. https://doi.org/ 10.2136/SSSAJ1980.03615995004400050002X.
- Yang, C., Sakai, M., Jones, S.B., 2013. Inverse method for simultaneous determination of soil water flux density and thermal properties with a penta-needle heat pulse probe. Water Resour. Res. 49, 5851–5864. https://doi.org/10.1002/wrcr.20459.
- Yu, A.B., An, X.Z., Zou, R.P., Yang, R.Y., Kendall, K., 2006. Self-assembly of particles for densest packing by mechanical vibration. Phys. Rev. Lett. 97, 265501 https://doi. org/10.1103/PHYSREVLETT.97.265501/FIGURES/4/MEDIUM.
- Zhang, M., Lu, Y., Ren, T., Horton, R., 2020. In-situ probe spacing calibration improves the heat pulse method for measuring soil heat capacity and water content. Soil Sci. Soc. Am. J. 84, 1620–1629. https://doi.org/10.1002/SAJ2.20124.